Nanosecond high-power dense microplasma switch for visible light

Cite as: Appl. Phys. Lett. **105**, 223501 (2014); https://doi.org/10.1063/1.4902914
Submitted: 28 July 2014 • Accepted: 16 November 2014 • Published Online: 01 December 2014

A. Bataller, J. Koulakis, S. Pree, et al.

Nanosecond high-power dense microplasma switch for visible light

A. Bataller,[a] J. Koulakis, S. Pree, and S. Putterman
Department of Physics and Astronomy, University of California Los Angeles, Los Angeles, California 90095, USA

(Received 28 July 2014; accepted 16 November 2014; published online 1 December 2014)

Spark discharges in high-pressure gas are known to emit a broadband spectrum during the first 10 s of nanoseconds. We present calibrated spectra of high-pressure discharges in xenon and show that the resulting plasma is optically thick. Laser transmission data show that such a body is opaque to visible light, as expected from Kirchoff's law of thermal radiation. Nanosecond framing images of the spark absorbing high-power laser light are presented. The sparks are ideal candidates for nanosecond, high-power laser switches. © *2014 AIP Publishing LLC*.
[http://dx.doi.org/10.1063/1.4902914]

A Planck blackbody spectrum is emitted from a cavitating gas bubble as its implosion reaches a minimum radius. Blackbody radiation from cavitation can be observed in a wide-ranging parameter space that includes temperatures as low as $\sim$1 eV and atomic densities as low as $\sim 10^{21}\,\mathrm{cm}^{-3}$.[1–5] These parameters can also be achieved in a spark discharge in a high-pressure gas. Furthermore, sparks have an advantage over sonoluminescence in that sparks can be triggered on demand. As blackbodies are opaque, experiments on sonoluminescence suggest using sparks in high-pressure gases as an active optical limiter for high-power visible light. Our goal of achieving blackbody behavior in non-cavitating systems is supported by the observed blackbody response in laser breakdown of high-pressure gases.[6] The opacity of high-pressure sparks at early times has been inferred from their broadband emission.[7] Here, we demonstrate a calibrated Planck spectrum and measure transmission under the above conditions. The experimental conditions employed in this letter lead to a nanosecond microplasma switch that is capable of high-power handling. A potential application that utilizes this opaque switching behavior is the protection of sensitive imaging devices from high-power lasers.

The application of high-voltage (HV) between two gas-separated electrodes can generate plasma through dielectric breakdown. This rapid breakdown is known as spark discharge. Sparks can be developed in nanosecond timescales and heated to thousands of degrees through time-varying resistive heating.[8] At these temperatures, gases become ionized and radiate light. This rapid increase of light emission is shown in Figs. 1(a) and 1(b) for sparks generated in high-pressure xenon gas. At high values of light emission, the plasma becomes more absorptive of the incoming light as plotted in Figs. 1(a) and 1(b). Figs. 1(c) and 1(d) show false color images (5 ns gate) of spark plasmas absorbing light from a 532 nm pulsed laser. For a system with temperature T, emission and absorption of light are related by Kirchhoff's law

$$\frac{J_\nu}{A_\nu} = S_\nu = \frac{2\pi h\nu^3}{c^2}\frac{1}{e^{h\nu/kT}-1}, \tag{1}$$

where J_ν is the amount of radiation emitted per unit time per unit surface area, A_ν is the absorptivity, and S_ν is the radiant energy flux of a blackbody at frequency ν. This law states that the ratio of a body's emission to its absorption is equal to blackbody emission, which only depends on T and ν. The attainment of the blackbody limit ($A_\nu = 1$) is suggested by Fig. 1 not only because transmission drops to zero but also because the transmission remains zero while the light emission continues to increase. A similar response has also been observed for laser breakdown studies in atmospheric pressure gases.[9] In general, plasma emission becomes more intense with increasing density. This trend is observed in Fig. 1 for 2 and 10 bar discharges. Similarly, the amount of transmitted laser energy decreases with increasing pressure. Eventually, a critical pressure is reached where the plasma becomes opaque[7] and laser transmission falls to zero. For pressures $\gtrsim$10 bar, laser pulses are completely blocked and absorption occurs only on the plasma's surface (Fig. 1(d)). From Eq. (1), the condition for opacity is given by $A_\nu = 1$ and therefore $J_\nu = S_\nu$. This states that an opaque body must emit blackbody radiation for a given frequency. The transmission curve for 10 bar discharges in Fig. 1(b) indicates complete absorption at 532 nm and must therefore radiate as a blackbody at 532 nm. To confirm this requirement, calibrated spectrum was measured as a function of time as shown in Fig. 2. For early moments, the discharge radiates a continuous broadband spectrum followed later in time by xenon line emission. Temporal line-outs from the spectral images are shown in Fig. 2(b). Indeed, this spectrum is well fit to blackbody emission (S_ν) during the same moments as complete laser absorption (Fig. 1(b)).

Spark discharges were generated using two tungsten needles (40 μm tip radius) centered in a stainless-steel pressure chamber (PC), as shown in Fig. 3(a). Optical access was granted with four UV fused-silica windows mounted on the PC. The distance between the electrode tips was 165 μm and adjusted using a custom high-pressure actuator. HV pulses were generated by an external circuit shown in Fig. 3(c). A variable-length fast pulser (Behlke FSWP71–02, 10 ns rise time) was charged with a +5 kV power supply through a 10 MΩ resistor. Upon triggering, +5 kV pulses were sent through a 1.36 m RG58C/U cable ending with a SHV

[a]Electronic address: bataller@physics.ucla.edu

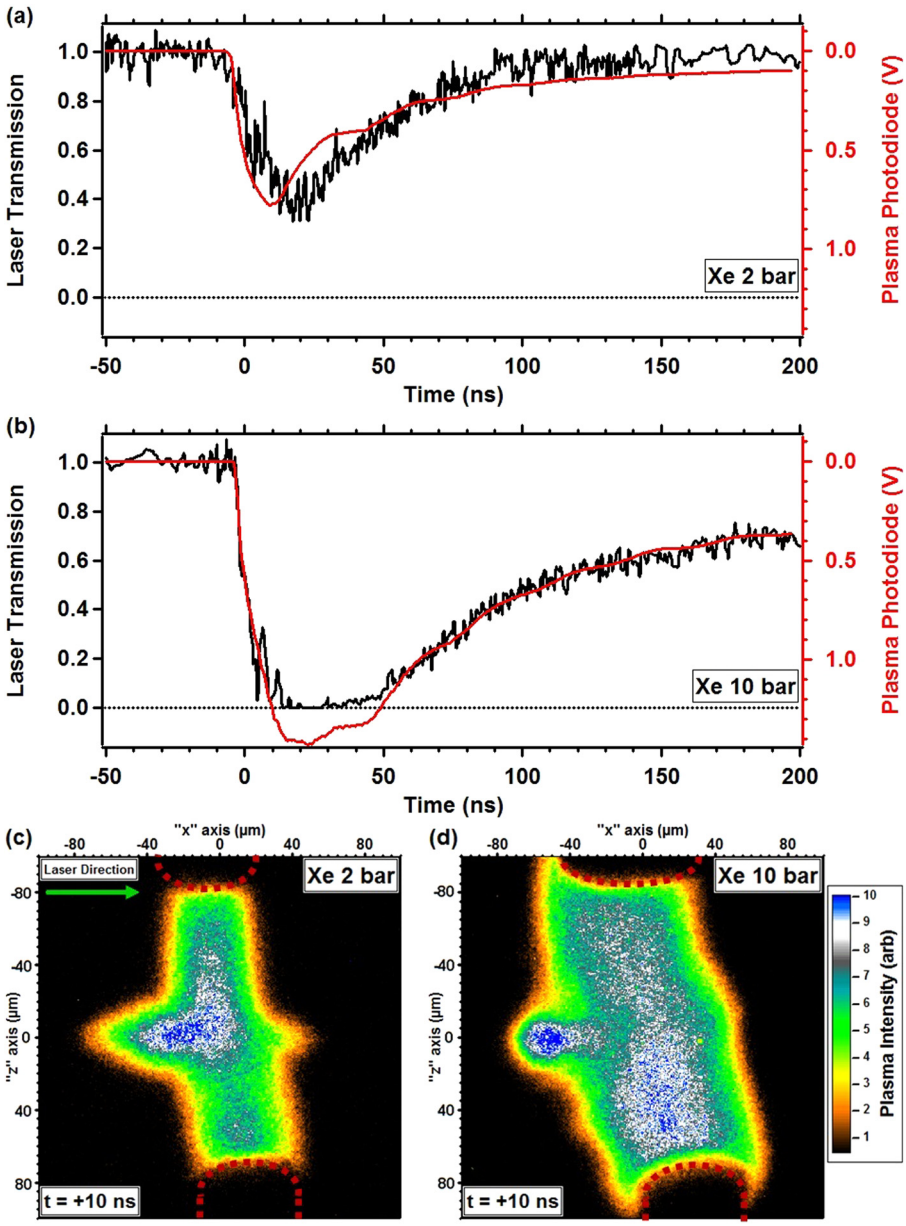

FIG. 1. Laser transmission and plasma emission of spark discharges formed in (a) 2 and (b) 10 bar xenon gas as a function of time. Laser transmission (black curve) was recorded for 532 nm laser pulses focused through the center of the spark plasma. Plasma emission (red curve) was recorded with a fast photodiode. False color images representing plasma light emission were taken with a framing camera during the moment of laser-plasma interaction for (c) 2 and (d) 10 bar discharges. Red dashed curves indicate the location of the HV electrodes. Laser pulses propagating from the left are absorbed by the spark volume and surface for 2 and 10 bar discharges, respectively. These transmission curves and images were obtained using laser intensities below the breakdown threshold.

connection. The HV electrode was connected to the external circuit through a SHV feed-through and the ground electrode was connected to the chamber body. The spark is achieved when the stray capacitance of the cable and electrodes charges to the breakdown threshold, as described in Ref. 10. Although pulse lengths were set to 1 μs for the discharges presented in this letter, the plasma is opaque for only the first ~50 ns. This timescale is set by a combination of circuit properties and the expansion of the heated gas.[11–13] Sparking was conducted at a rate of 5 Hz or slower to minimize any lingering effects of the previous shot. Due to the voltage being near the breakdown threshold, 10 bar discharges jittered in time by 100 s of nanoseconds relative to the input trigger. To improve the temporal jitter, seed electrons were created through the photoelectric effect by projecting a UV light source (deuterium lamp) onto the electrodes.[14]

The plasma images in Fig. 1 were acquired using a framing camera (Specialised-Imaging, Custom SIMD-052) capable of capturing four 3 ns images in a 12 ns interval. Following Fig. 3(b), plasma emission was collected by a Mitutoyo infinity-corrected microscope objective (MO) and imaged onto the framing camera with a tube lens (TL). The imaging system has a 10× magnification and a 2.0 μm spatial resolution. A filter stack (FS) was placed between the objective and tube lens. In FS3 were neutral density filters and a 532 nm notch filter (Stopline 532/1064 nm dual-notch) to protect the framing camera from incidental laser scattering and pass broadband plasma emission.

Laser transmission curves from Fig. 1 were measured by focusing laser pulses through the spark discharge. TEM00 pulses from a seeded YAG (Coherent Infinity) were focused into the PC (green arrows in Fig. 3(b)) with a 40 mm focal length objective (LO). The measured flashwidth, energy, beam waist, and peak focal intensity was 2.2 ± 0.15 ns, 8.0 ± 0.9 μJ/pulse, 9.5 ± 1.0 μm, and $1.9 \pm 0.4 \times 10^{10}$ W/cm^2, respectively. After passing through the spark discharge at minimum focus, the laser is collected, filtered, and imaged onto a triggerable CCD camera (Mightex CCE-B013-U). In FS1 were neutral density filters and a 532 nm line filter to protect the camera from strong laser intensities and block

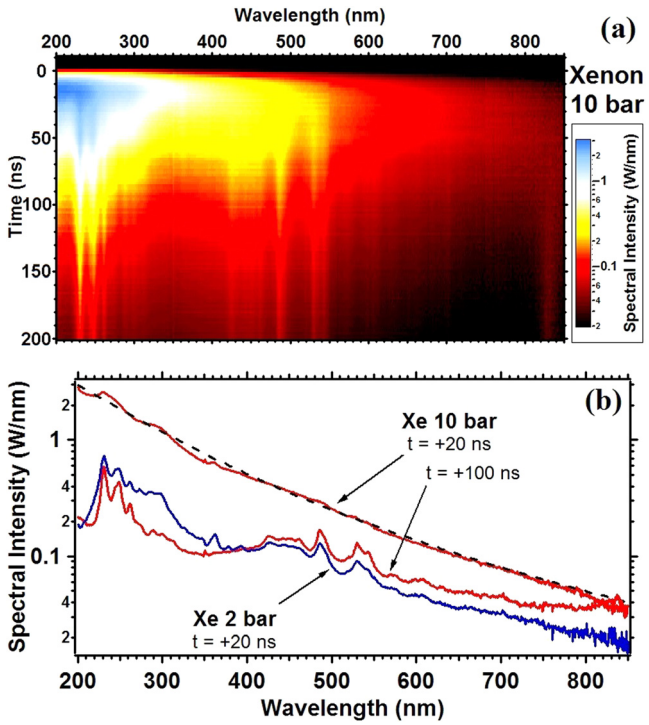

FIG. 2. Calibrated spectrum for 10 bar xenon discharges. (a) Temporally resolved spectral image shows continuous broadband emission for early times. As the plasma expands, xenon line emission emerges from the continuum for later times. (b) Spectral line-outs reveal opaque behavior during the early moments of discharge and is well fit to blackbody emission (black dashed curve, $T = 24000\,\mathrm{K}$ and $4.9 \times 10^4\,\mu\mathrm{m}^2$ blackbody emission area). Blackbody spectrum is observed concurrently with complete absorption from Fig. 1(b).

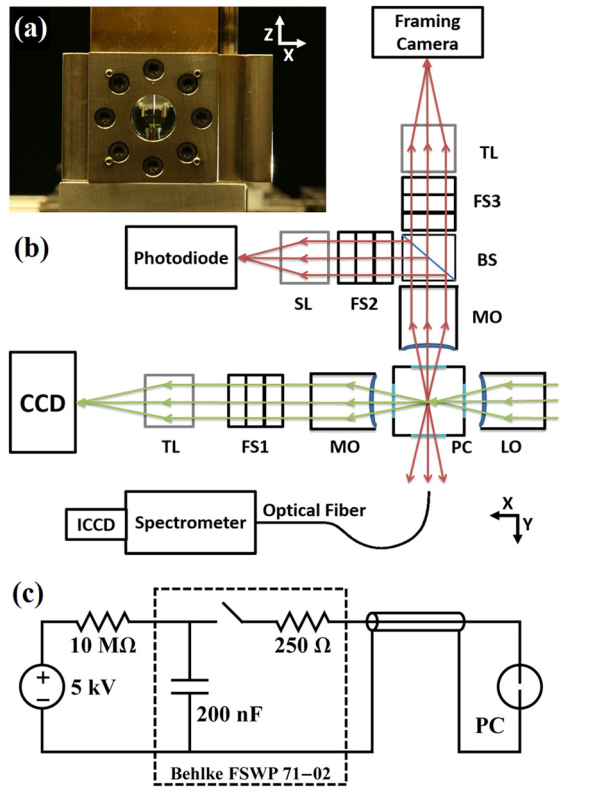

FIG. 3. Experimental setup: (a) Photograph of pressure chamber with tungsten needle electrodes. (b) Optical block diagram for measuring laser transmission and plasma emission, and for fast spark imaging (framing). Included are laser (green arrows) and plasma emission (red arrows) ray traces. A portion of the plasma emission is collected by an optical fiber and directed to a gated spectrometer. The x, y, and z axes are defined by the arrows in a) and b), the origin of which is taken to be the plasma center. (c) High-voltage circuit diagram.

broadband plasma emission. Transmission is normalized using the integrated laser intensity on the CCD for pulses arriving before the spark discharge.

Due to the spark's temporal jitter, a signal representing plasma emission ("Plasma Photodiode" in Fig. 1) was needed to sort the CCD and framing camera images as a function of time. As shown in Fig. 3(b), a 50:50 broadband beamsplitter sends a portion of the plasma emission to a fast photodiode (1 ns rise time). The broadband light sent to the photodiode was filtered by FS2 (532 nm notch) and demagnified 0.6× by a 25 mm focal length singlet lens (SL). Timing signals from the plasma photodiode and cameras were recorded on an oscilloscope for every laser pulse. A timestamp was assigned for each event based on the time difference between the plasma photodiode and the camera signals. Timing to each instrument was controlled through a delay generator (SRS DG645).

Temporally resolved spectrum was acquired using a calibrated fiber-coupled spectrometer (Acton SpectraPro 300i) and gated to 10 ns exposures with an ICCD (Princeton Instruments PI-MAX). Once more, a timestamp from the plasma photodiode is recorded for every discharge. In this way, spectra are sorted in time and averaged (2 ns time-bins) to make the spectral image in Fig. 2(a). Because the spectrum is calibrated in intensity, the fit in Fig. 2(b) provides both a blackbody temperature (24 000 K) and area of emission ($4.9 \times 10^4\,\mu\mathrm{m}^2$), with a fitting error of ~20%. This is in rough agreement with the plasma's luminous area ($2\pi Rh = 2\pi \times 40\,\mu\mathrm{m} \times 165\,\mu\mathrm{m} = 4.1 \times 10^4\,\mu\mathrm{m}^2$) taken from the framing camera images. For times $\gtrsim$50 ns, xenon lines emerge from the continuum and increase in strength. The appearance of these lines indicates a transparent plasma and is consistent with the absorption measurement in Fig. 1(b). This increase in line emission is due primarily to the plasma's hydrodynamic expansion into the surrounding gas, resulting in a lowered atomic density. For comparison, spectrum at 2 bar xenon discharge is provided in Fig. 2(b) and shows reasonable agreement.

Normalized transmission curves were constructed for peak laser intensities spanning 6 orders of magnitude (1.9×10^7–$10^{13}\,\mathrm{W/cm}^2$, Ref. 15). These curves were independent of laser intensity until the laser breakdown threshold was reached, indicating that the loss of laser light is due to linear absorption by the spark plasma. The laser breakdown threshold was measured at $7.7 \pm 1.5 \times 10^{11}\,\mathrm{W/cm}^2$ and $1.9 \pm 0.4 \times 10^{11}\,\mathrm{W/cm}^2$ for 2 and 10 bar, respectively (consistent with Ref. 16). Beyond the laser breakdown threshold, the transmission curves deviated toward lower transmission due to energy loss from laser breakdown.[17] This trend suggests that there is no limit to the plasma's power handling capability and can be utilized at very high laser intensities. To demonstrate this capability, Fig. 4 shows framing images of 10 bar spark-laser interactions for a laser intensity ten times larger than laser breakdown ($1.9 \times 10^{12}\,\mathrm{W/cm}^2$). Each image was exposed for 5 ns with 0 ns interframe time. In Fig. 4(a),

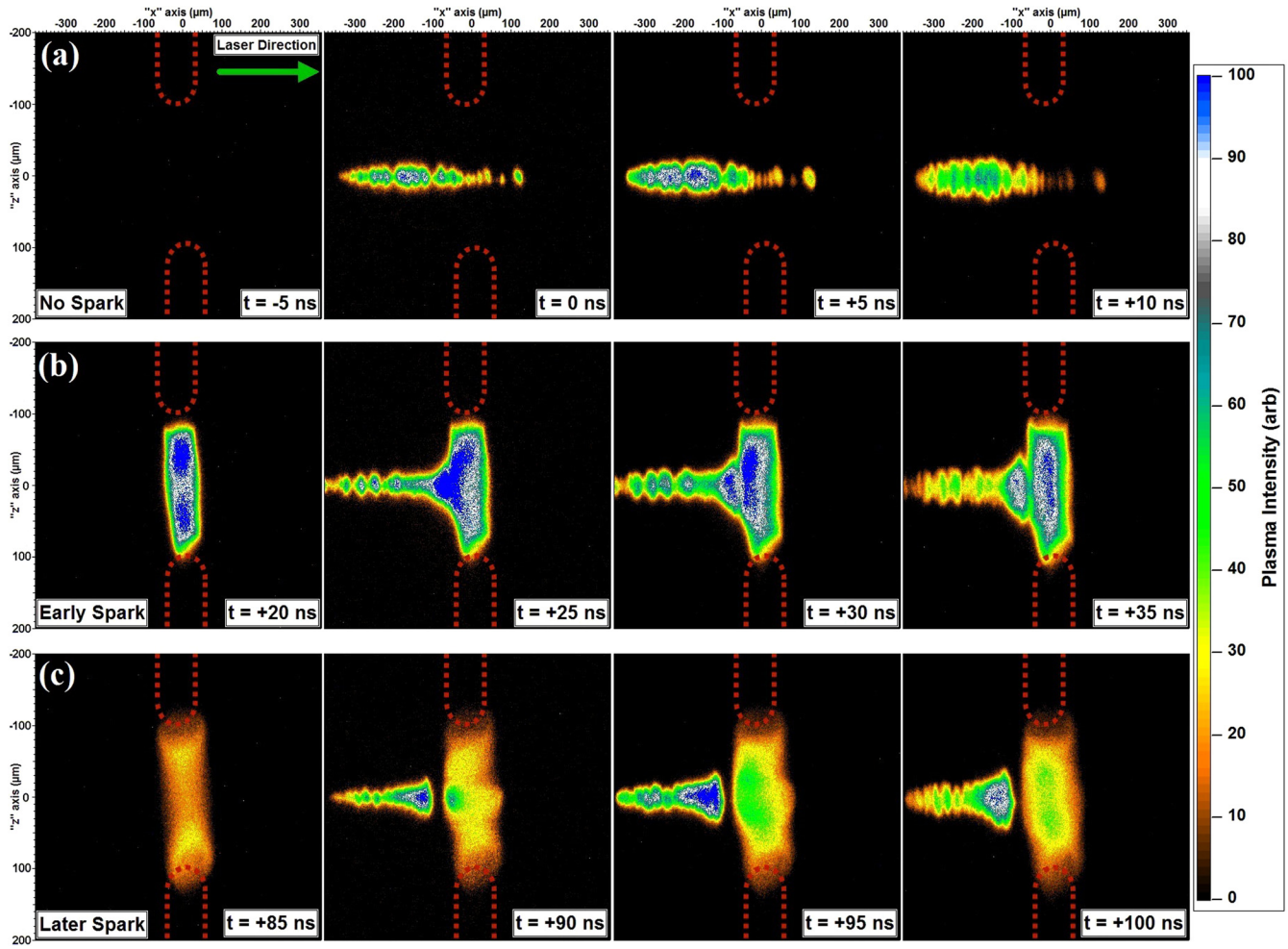

FIG. 4. 5 ns framing images (false color) of three individual events: (a) Laser breakdown without a spark and (b) laser absorption at +25 ns and (c) +90 ns after spark discharge initiation in 10 bar xenon gas. The timestamps given in (b) and (c) indicate the moment the image was taken relative to the spark discharge. For the case of (a) no spark, the image was taken relative to the arrival of the laser pulse. In all cases, the laser intensity (1.9×10^{12} W/cm^2) was set above the breakdown threshold and centered between the electrode gap. Laser arrival occurred during the second frame of each row and resulted in a laser-plasma interaction. Red dashed curves indicate the location of the HV electrodes. A dark region exists between the laser breakdown and spark plasma for $t \gtrsim 50$ ns and grows larger with later laser pulses. Shadowgraph measurements have shown this effect is due to laser breakdown induced by a shock front generated by the spark discharge. (Multimedia view) [URL: http://dx.doi.org/10.1063/1.4902914.1][URL: http://dx.doi.org/10.1063/1.4902914.2][URL: http://dx.doi.org/10.1063/1.4902914.3]

the incident laser pulse (from left to right) is focused between the tungsten electrodes with the spark switched off (no HV). In this configuration, laser breakdown is formed both before and after the electrodes, and ~25% of the laser energy is transmitted to the CCD camera. With the spark activated, the laser pulse is focused onto the plasma column and is completely absorbed (Fig. 4(b)). Once more, no laser energy passes through to the CCD camera for early times (~0–50 ns after spark initiation). Laser energy is absorbed only on the surface of the spark plasma, which further indicates an opaque body. The laser energy deposited to the spark plasma is so large that a luminous wave propagates within the plasma (from left to right in Fig. 4(b)). Conversely, laser energy is deposited to the plasma volume at later times as shown in Fig. 4(c). Here too a luminous wave propagates within the plasma (from middle to top/bottom in Fig. 4(c)). This observation is consistent with both the measured spectrum and absorptivity, as a volume emitter is also a volume absorber.

The nanosecond optical switch device presented in this letter was motivated by the observation of a dense plasma inside a sonoluminescing bubble. The dense microplasma exists at an unexpectedly low temperature and has its origin in collective processes in a strongly coupled plasma.[6] We have generated an opaque plasma using spark discharges in high-pressure xenon. As an active optical limiter, this plasma has seemingly limitless power handling, as laser energy is converted into higher temperature and more plasma. In other words, the switch reported in this letter cannot be damaged because it is already broken. This optical switch can now be optimized in parameter space for faster discharge speeds, lower energy consumption, and longer periods of opacity. In addition to device applications, the system discussed in this letter could lead to new probes of strongly coupled plasmas. By varying the density and other parameters typically inaccessible to sonoluminescence, new equations of state can be discovered for this exotic state of matter.

We gratefully acknowledge support from the Air Force Office of Scientific Research and DARPA MTO for

research on micro-plasmas. We thank Adam Collins, Brian Kappus, Brian Naranjo, and Guillaume Plateau for valuable discussions.

[1]D. J. Flannigan and K. S. Suslick, Nat. Phys. **6**, 598 (2010).
[2]B. Kappus, S. Khalid, A. Chakravarty, and S. Putterman, Phys. Rev. Lett. **106**, 234302 (2011).
[3]S. Khalid, B. Kappus, K. Weninger, and S. Putterman, Phys. Rev. Lett. **108**, 104302 (2012).
[4]B. Kappus, A. Bataller, and S. Putterman, Phys. Rev. Lett. **111**, 234301 (2013).
[5]A. Bataller, B. Kappus, C. Camara, and S. Putterman, Phys. Rev. Lett. **113**, 024301 (2014).
[6]A. Bataller, G. R. Plateau, B. Kappus, and S. Putterman, Phys. Rev. Lett. **113**, 075001 (2014).
[7]L. Michel and H. Fischer, Appl. Opt. **11**, 899 (1972).
[8]H. Fischer, J. Opt. Soc. Am. **51**, 543 (1961).
[9]V. Hohreiter, J. Carranza, and D. Hahn, Spectrochim. Acta B **59**, 327 (2004).
[10]T. Iwata, T. Tanaka, T. Komatsu, and T. Araki, Rev. Sci. Instrum. **71**, 4045 (2000).
[11]H. Fischer, J. Opt. Soc. Am. **47**, 981 (1957).
[12]H. Fischer and C. C. Gallagher, Appl. Opt. **4**, 1151 (1965).
[13]J. B. Higham and J. M. Meek, Proc. Phys. Soc., Sect. B **63**, 649 (1950).
[14]T. Komatsu, T. Iwata, and T. Araki, Rev. Sci. Instrum. **71**, 1621 (2000).
[15]See supplementary material at http://dx.doi.org/10.1063/1.4902914 for all 10 bar Xe transmission curves.
[16]D. I. Rosen and G. Weyl, J. Phys. D: Appl. Phys. **20**, 1264 (1987).
[17]C. V. Bindhu, S. S. Harilal, M. S. Tillack, F. Najmabadi, and A. C. Gaeris, J. Appl. Phys. **94**, 7402 (2003).